

# JGR Atmospheres

## RESEARCH ARTICLE

10.1029/2021JD035982

### Special Section:

SOUTHTRAC-GW: An Airborne Field Campaign to Explore Gravity Wave Dynamics at the World's Strongest Hotspot

### Key Points:

- First latitudinal comparison of mesosphere and lower thermosphere momentum fluxes along the Andes mountain range
- 28-day mean momentum flux dynamics vary depending on the latitude and the season
- Total momentum flux distributions are well represented by log-normal functions, with parameters varying on location and season

### Correspondence to:

J. F. Conte,  
[conte@iap-kborn.de](mailto:conte@iap-kborn.de)

### Citation:

Conte, J. F., Chau, J. L., Liu, A., Qiao, Z., Fritts, D. C., Hormaechea, J. L., et al. (2022). Comparison of MLT momentum fluxes over the Andes at four different latitudinal sectors using multistatic radar configurations. *Journal of Geophysical Research: Atmospheres*, 127, e2021JD035982. <https://doi.org/10.1029/2021JD035982>







Received 5 OCT 2021

Accepted 12 JAN 2022

© 2022. The Authors.

This is an open access article under the terms of the [Creative Commons Attribution-NonCommercial-NoDerivs License](#), which permits use and distribution in any medium, provided the original work is properly cited, the use is non-commercial and no modifications or adaptations are made.

## Comparison of MLT Momentum Fluxes Over the Andes at Four Different Latitudinal Sectors Using Multistatic Radar Configurations

J. Federico Conte<sup>1</sup> , Jorge L. Chau<sup>1</sup> , Alan Liu<sup>2</sup> , Zishun Qiao<sup>2</sup> , David C. Fritts<sup>3</sup> , José L. Hormaechea<sup>4,5</sup> , Jacobo O. Salvador<sup>5,6</sup>, and Marco A. Milla<sup>7,8</sup>

<sup>1</sup>Leibniz Institute of Atmospheric Physics at the University of Rostock, Kühlungsborn, Germany, <sup>2</sup>Embry-Riddle Aeronautical University, Daytona Beach, FL, USA, <sup>3</sup>GATS Inc., Boulder, CO, USA, <sup>4</sup>Facultad de Ciencias Astronómicas y Geofísicas, UNLP, La Plata, Argentina, <sup>5</sup>CONICET, Buenos Aires, Argentina, <sup>6</sup>Universidad Nacional de la Patagonia Austral, Río Gallegos, Argentina, <sup>7</sup>Radio Observatorio de Jicamarca, Instituto Geofísico del Perú, Lima, Peru, <sup>8</sup>Sección Electricidad y Electrónica, Pontificia Universidad Católica del Perú, Lima, Peru

**Abstract** The middle atmosphere over South America, particularly above the Andes mountain range, is known as one of the most dynamically active regions in the world. Previous studies have investigated wave dynamics at mesosphere and lower thermosphere (MLT) altitudes within this region, but only a handful of them have made use of continuous measurements provided by specular meteor radars (SMRs). Furthermore, it was only until recently that MLT horizontal wind gradients were estimated for the first time using Spread Spectrum Interferometric Multistatic meteor radar Observing Network (SIMONe) Argentina, a multistatic SMR network located in southern Patagonia. By observing larger amounts of meteors from different viewing angles, multistatic SMRs allow, among others, for more reliable momentum flux estimates. In this work, we explore and compare the summer and winter MLT momentum flux dynamics at low and middle latitude sectors over the Andes mountain range. We also investigate the intermittency of the total momentum flux over these sectors. For this purpose, we analyze measurements provided by four multistatic SMR networks: SIMONe Peru (12°S), CONDOR (30°S), SIMONe Argentina (49°S) and MMARIA-SAAMER (54°S). We find that the momentum flux dynamics can change considerably over distances of only a few hundred km (e.g., southern Argentina). On the other hand, the contributions of large momentum fluxes to the total flux can be similar between regions separated by thousands of km (e.g., between Peru and southern Argentina).

## 1. Introduction

Gravity waves (GWs) are one of the main drivers of the dynamics of the neutral atmosphere (Andrews et al., 1987; Fritts & Alexander, 2003; Holton, 2004). By transporting and depositing momentum and energy at different altitude regions, they contribute significantly to different atmospheric processes, such as the summer-to-winter pole mesospheric circulation, the quasi-biennial oscillation, etc. (e.g., Garcia & Boville, 1994; Sato & Dunkerton, 1997). Gravity waves are of intermittent nature (e.g., Geldenhuys et al., 2021). Both their sources and the medium in which they propagate introduce patchy features in the spatial and temporal distributions of GWs. This intermittency can in turn affect atmospheric phenomena on a global scale (e.g., Yiğit et al., 2021). Thus, incorporating the effects of GWs into global circulation models has become a crucial task in order to better understand the Earth's climate (e.g., Morgenstern et al., 2010). One way to accomplish this task is to increase the amount of observational studies so as to reproduce the entire GW spectrum (e.g., Stephan et al., 2019).

Observations made by different satellite missions have been used to investigate GW climatologies and momentum fluxes (e.g., Ern et al., 2004; Preusse et al., 2002; Wu, 2001). However, satellite measurements have at least one drawback: they can only capture the effects of gravity waves with large horizontal scales (>600–700 km). At mesosphere and lower thermosphere (MLT) altitudes, mesoscale gravity wave momentum fluxes have been investigated using HF radars (e.g., Thorsen et al., 1997; Vincent & Reid, 1983). Hocking (2005) modified and extended to specular meteor radar (SMR) systems the multi-beam approach implemented in HF radars to extract information on momentum fluxes. Since then, many studies have used SMRs to explore momentum flux dynamics at altitudes between ~80 and 100 km (e.g., Andrioli et al., 2013; de Wit et al., 2016; Fritts et al., 2012; Placke et al., 2011; Spargo et al., 2019, and references therein).



**Figure 1.** Map showing the locations of (from north to south): SIMONe Peru (12°S), CONDOR (30°S), SIMONe Argentina (49°S) and MMARIA-SAMER (54°S). The concentric circumferences are centered at the transmitting sites, and indicate the regions of 50, 100 and 200 km radius. Map adapted from Google Earth.

The middle atmosphere above the South American Andean sector constitutes one of the most dynamically active regions in the world. However, it has been poorly investigated, mainly due to logistics problems to install remote sensors. A few studies have used (almost) continuous SMR measurements in order to investigate momentum flux dynamics, but only at the southern tip of the South American continent (e.g., Conte et al., 2021; de Wit et al., 2017; Fritts, Janches, Iimura et al., 2010; Stober et al., 2021). And just one of these studies took advantage of multistatic SMR measurements (Conte et al., 2021). By observing more meteors from different viewing angles, multistatic SMRs can provide more reliable information on the variability of mesoscale GW-driven momentum fluxes. Thus, with the purpose of answering questions such as, how much do momentum fluxes vary with latitude and season over South America? We set to explore observations made by four multistatic specular meteor radar networks recently installed at different locations near the Andes mountain range. A comparison of the momentum fluxes at these four different latitudinal sectors of the South American continent is made for the first time. Preliminary results on the intermittency of the total momentum flux are also presented.

The paper is structured as follows. Section 2 describes the four multistatic systems considered in this study. Section 3 provides a description of the method employed to estimate the momentum fluxes from the radar measurements. The results are presented in Section 4 and discussed in Section 5. Concluding remarks are given in Section 6.

## 2. Specular Meteor Radar Networks

Measurements made by four different multistatic specular meteor radar networks have been used in this study to explore momentum fluxes at MLT altitudes over different sectors of the Andes mountain range (see Figure 1). In this section, a brief description of the four systems is provided, and a summary of the main technical aspects of each system is given in Table 1.

### 2.1. SIMONe Argentina

Spread Spectrum Interferometric Multistatic meteor radar Observing Network (SIMONe) systems constitute a novel way to materialize the concept called Multi-static Multi-frequency Agile Radar for Investigations of the Atmos-

phere (MMARIA) (e.g., Stober & Chau, 2015). Particularly, SIMONe Argentina is comprised of one single transmitting site with five linearly polarized Yagi antennas in a pentagon configuration, and five receiving sites with one single dual-polarization Yagi antenna. The receiving sites are located within an area of ~270 km of radius around the transmitting site, which situates in the town of Tres Lagos, Santa Cruz, Argentina (49.6°S, 71.4°W). SIMONe Argentina uses spread spectrum on transmission. Five different pseudo-random codes are generated at

**Table 1**

*Summary of Technical Details of the Four Multistatic Specular Meteor Radar (SMR) Networks Considered in This Study*

Multistatic SMR	SIMONe Peru	CONDOR	SIMONe Argentina	MMARIA-SAMER
Coordinates of transmitter	11.9°S, 76.8°W	30.2°S, 70.7°W	49.6°S, 71.4°W	53.8°S, 67.7°W
Number of links	5	3	5	3
Frequency (MHz)	32.55	35.15	32.55	32.55
Power (kW)	2 (AP)	48 (PP)	2 (AP)	64 (PP)
Method	Spread spectrum	Pulsed	Spread spectrum	Pulsed

*Note.* PP, Peak Power; AP, Average Power.

the transmitting site, and later on simultaneously decoded at each receiving site by means of compressed sensing (e.g., Urco et al., 2019). SIMONe Argentina operates at a frequency of 32.55 MHz, with an average power of 2000 W. For more details on this system, the reader is referred to Chau et al. (2021); Conte et al. (2021).

## 2.2. SIMONe Peru

SIMONe Peru has the same characteristics as SIMONe Argentina. The transmitting site is located at the Jicamarca Radio Observatory, Peru (11.9°S, 76.8°W), and the five receiving sites are distributed between 30 and 250 km around Jicamarca. For details on this system, the reader is referred to Chau et al. (2021). Both SIMONe Peru and SIMONe Argentina were installed in the last trimester of 2019, and are operated by the Leibniz Institute of Atmospheric Physics at the University of Rostock, Germany.

## 2.3. CONDOR

The Chilean Observation Network De MeteOr Radars (CONDOR) is a three-link pulsed ATRAD Ltd. system that was installed in Chile between June 2019 and February 2020. It comprises one transmitting/receiving site located at the Andes Lidar Observatory, or ALO (30.2°S, 70.7°W), a second receiving site roughly 130 km north of ALO, and a third receiving site located ~100 km to the south of ALO. Transmission is done at a frequency of 35.15 MHz with a peak output power of 48 kW. The CONDOR system is supported by the United States National Science Foundation (NSF). Further information can be found on the website <http://lidar.erau.edu/>.

## 2.4. MMARIA-SAAMER

The Southern Argentina Agile Meteor Radar (SAAMER) is a pulsed Genesis Ltd. SMR that transmits at a frequency of 32.55 MHz, with a peak output power of 64 kW (e.g., Fritts, Janches, Hocking, 2010; Janches et al., 2015). It is located in Rio Grande, Tierra del Fuego, Argentina (53.8°S, 67.7°W), and it has been operating since 2008. In April/May 2019, two ATRAD Ltd. receiving systems that consist of five two-element crossed Yagi antennas each, were installed in Tierra del Fuego. The purpose of this was to extend the coverage of SAAMER and upgrade the system to one with multi-static capabilities. One of the sites locates in the city of Ushuaia (54.8°S, 68.3°W), and it has been operating since May 2019. The second receiving site was installed next to the city of Tolhuin, in an area with no access to the main power grid. For this reason, it has only operated in a campaign basis during some weeks of 2019. The network comprising SAAMER and the two added receiving sites is called MMARIA-SAAMER, and constitutes the first realization in the southern hemisphere of the MMARIA concept with a pulsed system.

## 3. Data Analysis

In this work, the procedure introduced by Hocking (2005) was implemented in order to extract information about MLT vertical momentum fluxes from the observations provided by the above-mentioned four multistatic SMR networks. Briefly, this means fitting the following equation to all the meteor observations made within a given time-altitude bin

$$(\mathbf{u}' \cdot \mathbf{k})^2 = (2\pi(f - \hat{f}))^2. \quad (1)$$

Here,  $\mathbf{k}$  and  $f$  are, respectively, the Bragg wave vector (scattered minus incident wave vectors) and the measured Doppler shift for each meteor detection, and  $\mathbf{u}'$  represents the perturbed wind vector (unknown).  $\mathbf{k}$  is determined considering the World Geodetic System 1984, or WGS84 (e.g., Chau & Clahsen, 2019; Stober et al., 2018), and  $\hat{f}$  is a mean Doppler shift that is derived using

$$\hat{f} = \mathbf{u} \cdot \mathbf{k} / 2\pi, \quad (2)$$

where  $\mathbf{u} = (u, v, w)$  is the mean wind vector obtained after solving  $\mathbf{u} \cdot \mathbf{k} = 2\pi f$ , in bins of 4 hr, 4 km (in altitude), shifted by 30 min and 1 km, respectively. The same binning was taken into consideration when solving for the six unknowns of Equation 1,  $\langle u'u' \rangle$ ,  $\langle v'v' \rangle$ ,  $\langle u'w' \rangle$ ,  $\langle v'w' \rangle$ ,  $\langle u'v' \rangle$  and  $\langle w'w' \rangle$ . However, the latter were



Zonal wind, diurnal and semidiurnal tides (28-day average)

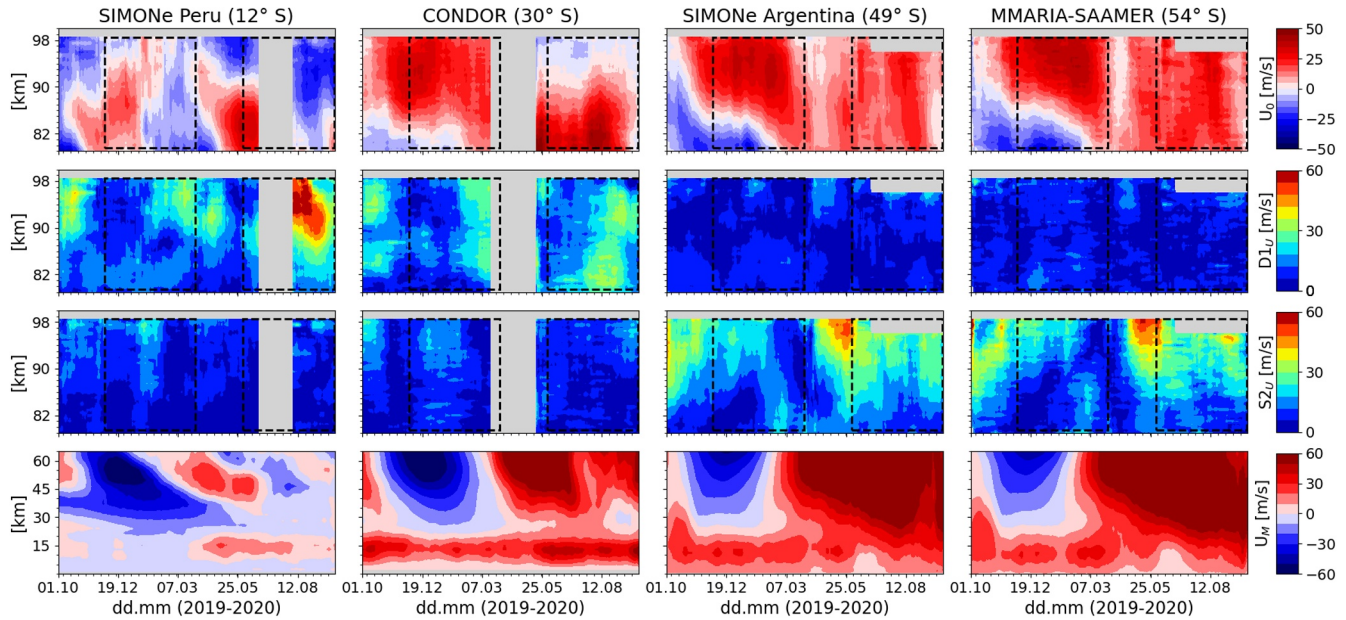


**Figure 2.** 28-day mean zonal wind ( $U_0$ ), diurnal ( $D1_u$ ) and semidiurnal ( $S2_u$ ) tides, and MERRA-2 mean zonal wind ( $U_M$ ), from 1 October 2019 until 30 September 2020 for (first column) SIMONE Peru (second column) CONDOR, (third column) SIMONE Argentina, and (fourth column) MMARIA-SAAMER. The gray areas indicate either data gaps or removed artifacts that resulted from the 28-day averaging. The black dashed rectangles highlight the time and altitude intervals in which the momentum fluxes have been analyzed. In case of MERRA-2 data, altitudes are approximate. To highlight the differences in the amplitudes, different colorbar magnitudes have been used for  $U_0$  and  $U_M$ .

estimated only in those bins containing 40 meteor detections or more. Both the mean winds and the momentum fluxes were estimated using only those meteor detections with corresponding zenith angles less than  $60^\circ$ . To minimize the effects of different meteor distributions due to the distinct geometries of the systems, a horizontal circle of 200 km radius centered at the transmitting site was considered for all the systems. The vertical component ( $w$ ) of the wind vector  $\mathbf{u}$  was assumed to be equal to zero in the mean wind estimation process.

It should be noted that because the subtracted mean Doppler shifts in Equation 1 were estimated using 4 hr, 4 km mean horizontal winds, the momentum flux estimates hereafter presented are representative of waves with periods shorter than 4 hr and vertical wavelengths of 4 km or less. The horizontal scales are in the order of 400 km or less. This is because the 4 hr, 4 km mean winds comprise waves with horizontal scales of 400 km or more, periods of 4 hr or more, and vertical wavelengths larger than 4 km. Thus, after subtracting these mean winds (converted to Doppler shifts using Equation 2), what remains is the contribution of waves with scales and periods that are smaller than the values aforementioned.

## 4. Results

### 4.1. Mean Winds and Tides

To provide context for the subsequent discussion on our momentum flux estimates, results on mean horizontal winds and the dominant tidal components are presented first. Figure 2 shows 28-day mean zonal winds ( $U_0$ ), and 28-day zonal components of the solar diurnal ( $D1_u$ ) and semidiurnal ( $S2_u$ ) tides over (from left to right) SIMONE Peru, CONDOR, SIMONE Argentina and MMARIA-SAAMER. The bottom row is used to present 28-day averages of Modern-Era Retrospective analysis for Research and Applications, Version 2 (MERRA-2) mean zonal winds ( $U_M$ ) at the grid points closest to the actual locations of the transmitting sites of each multistatic SMR network. The four parameters are in units of m/s, and the altitudes are given in km. The latter are approximate in the case of MERRA-2 data. Figure 3 shows the same quantities, but for the case of the meridional component.

## Meridional wind, diurnal and semidiurnal tides (28-day average)

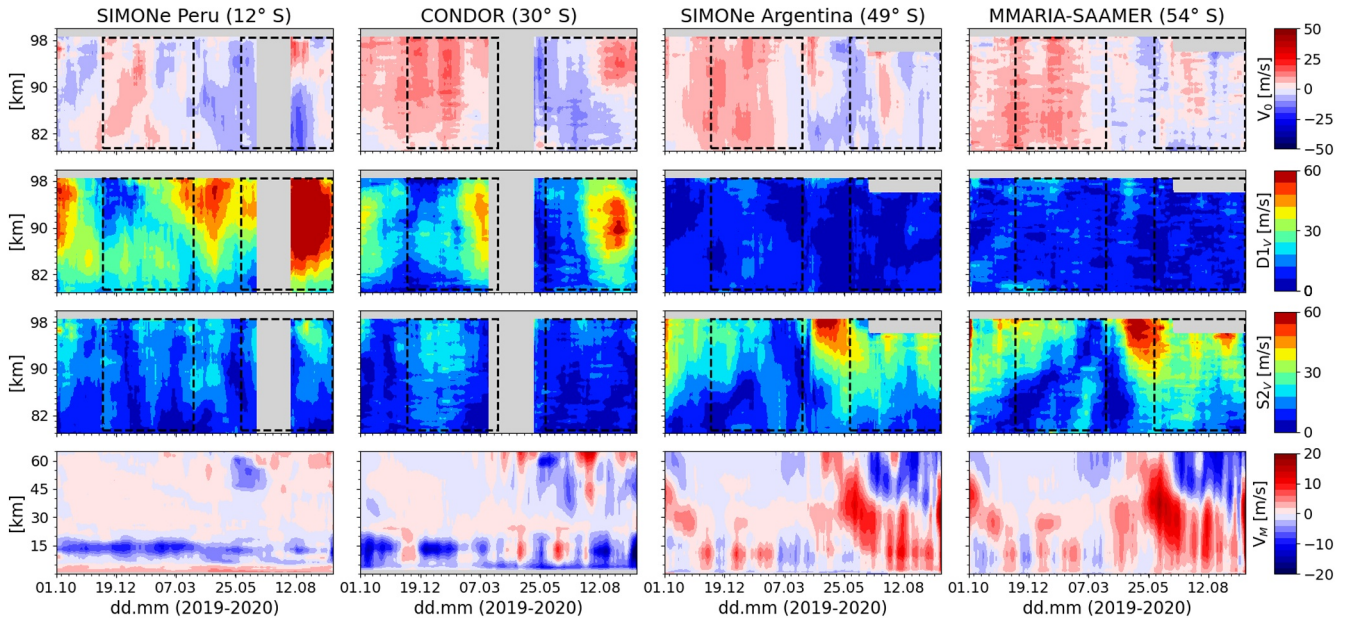


**Figure 3.** Same as Figure 2, but for the meridional component. Again notice that, in order to highlight the differences in their amplitudes, different colorbar magnitudes have been used for  $V_0$  and  $V_M$ .

The mean winds and tides presented in Figures 2 and 3 were obtained after fitting SMR hourly horizontal winds with a truncated Fourier series by means of a least squares technique (e.g., Conte et al., 2019; Sandford et al., 2006; Stening et al., 1997). The fitting procedure was carried out using a running bin of 28 days and 4 km (in altitude), shifted by 1 day and 1 km, respectively. This specific bin size was selected with the purpose of extracting mean winds and tides with similar time-altitude variability as that of the momentum fluxes (see next Section).  $U_M$  ( $V_M$ ) values were obtained after computing a 28-day running mean shifted by 1 day of 3-hourly MERRA-2 zonal (meridional) winds at each pressure level. Pressure levels were converted to heights considering a scale height equal to 8 km.

From Figure 2, it can be seen that mean zonal winds in the MLT are different both in time and altitude between SIMONE Peru and CONDOR. During (southern hemisphere) late spring and summer, CONDOR mean zonal winds exhibit considerable similarities with the mean zonal winds observed over SIMONE Argentina and MMARIA-SAAMER. Above these last two, the mean zonal winds behave very similarly all year long. Notice that the height of the mean zonal wind summer reversal decreases with the latitude, as previously shown in other studies (e.g., Conte et al., 2018; Wilhelm et al., 2019). An analogous comparison can be done in the case of MERRA-2 mean zonal winds. Over SIMONE Argentina and MMARIA-SAAMER,  $U_M$  exhibits similar characteristics, with strong eastward jets during the winter, and dominant westward winds during the summer, at upper stratosphere and lower mesosphere altitudes. At CONDOR, the summer westward mean zonal winds have stronger amplitudes, and the winter eastward jets are weaker, compared to SIMONE Argentina and MMARIA-SAAMER. MERRA-2 mean zonal winds are considerably different over SIMONE Peru, in comparison to the other three locations. With the exception of SIMONE Peru, the continuity in the vertical transition from MERRA-2 to SMR mean zonal winds is remarkably good. The only noticeable difference lies in the amplitudes, with MERRA-2 mean zonal winds being roughly 10–20 m/s stronger than those obtained from SMR measurements.

The  $D1_u$  tidal component dominates at both SIMONE Peru and CONDOR, while  $S2_u$  is the tide that dominates over SIMONE Argentina and MMARIA-SAAMER. This is not surprising, since it is known that the diurnal tide is the strongest tidal wave at low latitudes, and the semidiurnal tide prevails at middle latitudes (e.g., Andrews et al., 1987; Oberheide et al., 2009; Pancheva & Mukhtarov, 2011). As it was in the case of the mean zonal wind, the  $S2_u$  tide has similar characteristics at 49°S and 54°S, with the strongest amplitudes observed above ~93 km during late autumn and the beginning of the winter. The  $D1_u$  tide at both SIMONE Peru and CONDOR, enhances

### Mom. flux (28-d average) / Summer season

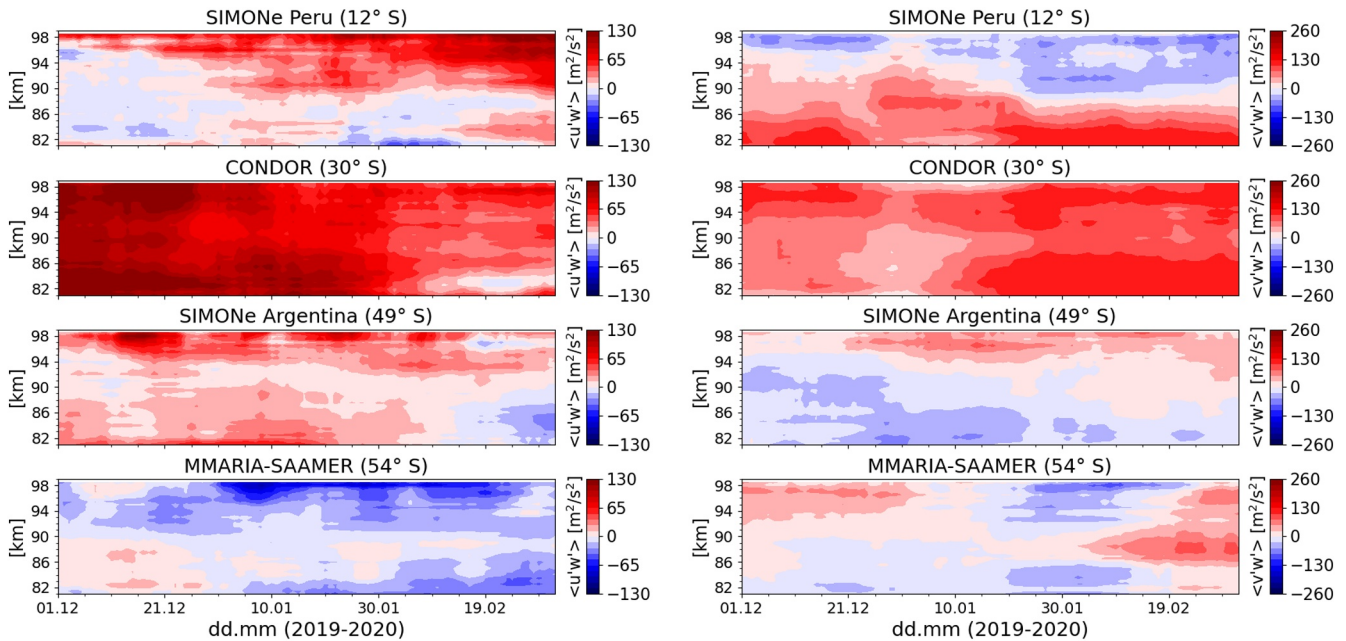


**Figure 4.** 28-day averages of (left) zonal and (right) meridional vertical momentum fluxes between 1 December 2019 and 31 March 2020. The momentum fluxes were estimated after subtracting 4 hr, 4 km (in vertical) mean horizontal winds. Data gaps are indicated in white. Notice that the colorbar magnitudes are different for the zonal and meridional components.

during the same periods of the year, although it does this with stronger amplitudes over SIMONE Peru. Maximum amplitudes of  $D1_u$  are observed during the winter, and they reach lower altitudes over CONDOR.

The diurnal and semidiurnal tides exhibit similar features in the case of the meridional component (see Figure 3). The main difference is in the amplitudes: both  $D1_v$  and  $S2_v$  have amplitudes 10–20 m/s larger than their zonal counterparts. Another difference can be noticed in the case of  $D1_v$ . The maximum amplitudes of this tidal component reach lower altitudes over SIMONE Peru, and not at CONDOR.  $S2_v$  develops considerable amplitudes not only in the fall, but also during most of the wintertime at both SIMONE Argentina and MMARIA-SAAMER.

The mean meridional winds over SIMONE Argentina and MMARIA-SAAMER are very similar. An equatorward  $V_0$  dominates during the summer, and a mix of equatorward and poleward  $V_0$  values are observed during the winter. Some continuity in the vertical transition from  $V_M$  to  $V_0$  can be observed at these two locations during the winter, but not in the summer, when  $V_M$  at mesosphere altitudes is predominantly poleward, but the SMR mean meridional winds blow toward the equator. Over SIMONE Peru and CONDOR, both  $V_0$  and  $V_M$  behave differently, although some similarities can be appreciated in the case of  $V_0$  during the second half of the winter. Notice that, as it was in the case of  $U_0$ , the mean meridional wind over CONDOR during the winter is similar to that observed over SIMONE Argentina and MMARIA-SAAMER. In contrast to the case of the mean zonal wind, the values of  $V_M$  are weaker than those of  $V_0$  at the four locations.

#### 4.2. Mean Momentum Fluxes

Results on the zonal ( $\langle u'w' \rangle$ ) and meridional ( $\langle v'w' \rangle$ ) vertical momentum fluxes are presented hereunder. Figure 4 shows 28-day averages of  $\langle u'w' \rangle$  on the left panels, and of  $\langle v'w' \rangle$  on the right ones. The plots correspond to the period 1 December 2019–31 March 2020, over (from top to bottom) SIMONE Peru, CONDOR, SIMONE Argentina and MMARIA-SAAMER. The units are in  $\text{m}^2/\text{s}^2$ . Data gaps are indicated in white. Figure 5 shows the same estimates, but for the period 1 June 2020–30 September 2020 (southern hemisphere winter season).

The 4-hr, 4-km momentum fluxes,  $\langle u'w' \rangle$  and  $\langle v'w' \rangle$ , were averaged using a 28-day running window, shifted by 1 day, in order to reduce their statistical uncertainties to values of less than 10%–15% (e.g., Conte et al., 2021;



### Mom. flux (28-d average) / Winter season

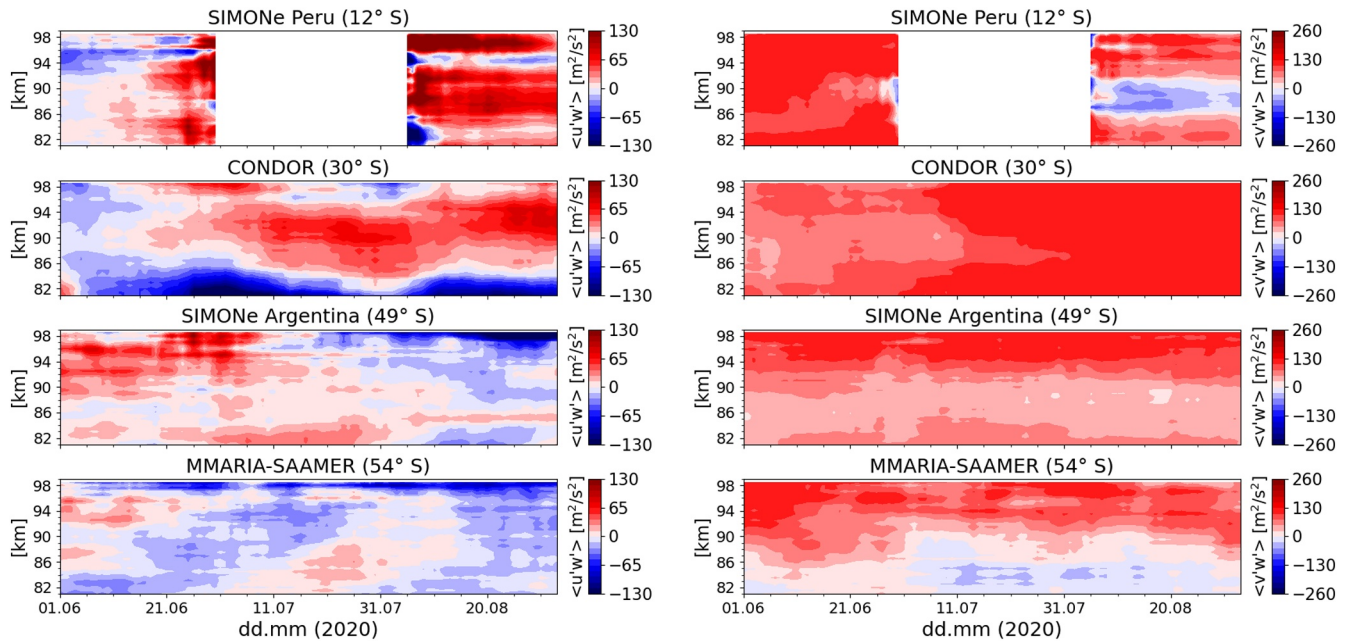


**Figure 5.** Same as Figure 4, but for the period 1 June 2020–30 September 2020 (southern hemisphere Winter season). Notice that the colorbar magnitudes are different for the zonal and meridional components.

Kudeki & Franke, 1998). It is of importance not to confuse the statistical uncertainties with the measurement errors propagated by the mathematical procedure used to estimate the momentum fluxes. The statistical uncertainties contain information about the (random and unresolved) geophysical variability of the observed atmosphere. By averaging over intervals of time longer than 25 days, one can significantly reduce the impact of the geophysical variability at MLT altitudes, and hence consider the momentum flux estimates as representatives of the mean momentum deposited by waves of horizontal scales less than  $\sim 400$  km.

There are at least five features that stand out from Figures 4 and 5: (a) the momentum flux dynamics are different among the four locations, particularly in the case of  $\langle u'w' \rangle$  during the summer; (b)  $\langle v'w' \rangle$  has stronger amplitudes than  $\langle u'w' \rangle$  at the four locations; (c) momentum fluxes exhibit the largest amplitudes over CONDOR during the summer, and (d) over SIMONE Peru during the winter season; and (e) momentum fluxes over CONDOR show little variability both in time and altitude during summer.

Between December and March above  $\sim 90$  km of altitude,  $\langle u'w' \rangle$  is mostly dominated by positive values at three of the four locations. Only MMARIA-SAAMER exhibits a dominance of negative values in  $\langle u'w' \rangle$ . Starting around the second week of January, between  $\sim 88$ – $90$  km of altitude over MMARIA-SAAMER,  $\langle u'w' \rangle$  shows a transition from negative to positive values, to then change again to negative ones above  $90$  km. A similar double transition is also observed in  $\langle v'w' \rangle$  above SIMONE Peru. But in this case, it happens during the winter, from positive to negative values, and again to positive ones above  $\sim 92$  km of altitude. CONDOR does not show this type of transitions, but rather mainly positive values for both  $\langle u'w' \rangle$  and  $\langle v'w' \rangle$  during both seasons and at all heights, except below  $\sim 87$  km for almost the entire winter, and above  $\sim 95$  km during some winter weeks. At SIMONE Argentina, a double transition can be observed in  $\langle u'w' \rangle$  during August 2020, around  $86$  km of altitude. Besides,  $\langle u'w' \rangle$  exhibits considerable variability in time and altitude, during both summer and winter seasons. In the case of  $\langle v'w' \rangle$ , its behavior during the winter is similar to that observed at CONDOR, with strong positive amplitudes over the entire height range.

During the summer,  $\langle u'w' \rangle$  estimates above  $\sim 90$  km of altitude over SIMONE Peru show values with opposite sign to those of the mean zonal wind. A similar behavior is observed in  $\langle v'w' \rangle$ , which presents mostly positive values at altitudes where the mean meridional wind is southward directed. The case of CONDOR is different. During the summer, and despite the strong vertical gradient present in the mean zonal wind,  $\langle u'w' \rangle$  remains

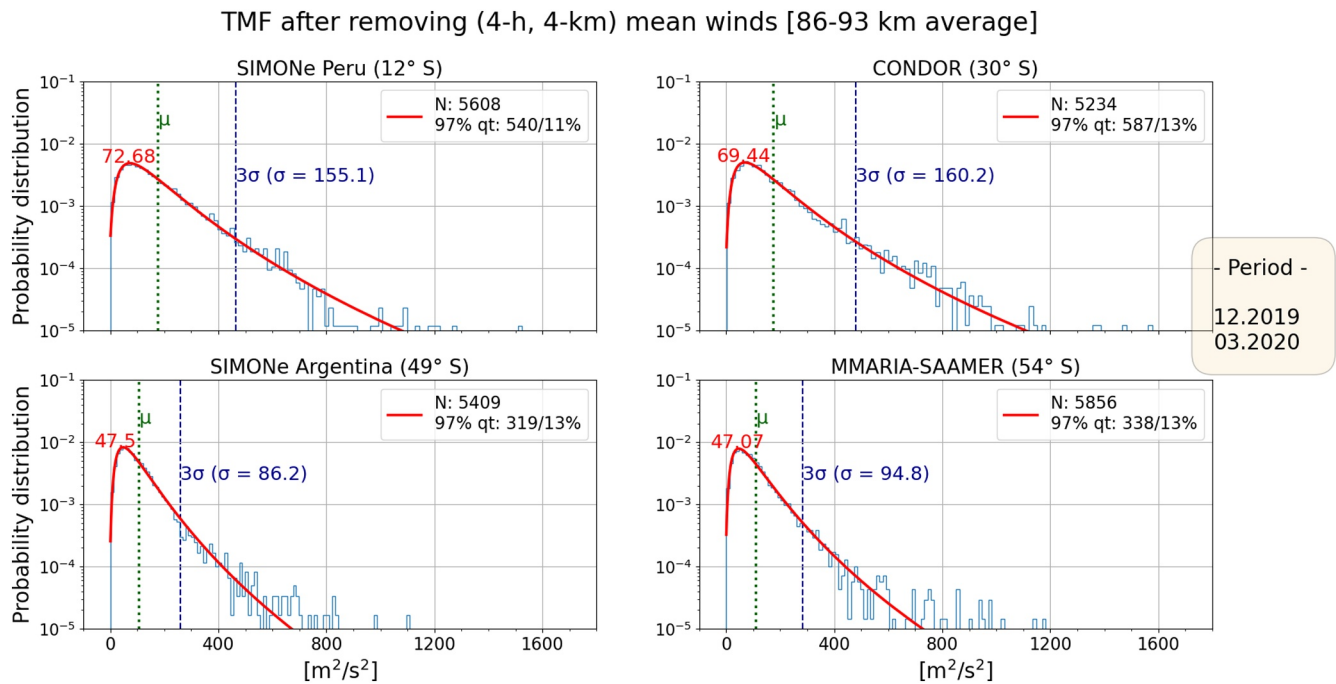


**Figure 6.** Total momentum flux probability distributions during the southern hemisphere summer season. The red curve corresponds to a log-normal function fitted to the measured distributions. The green vertical dotted line indicates the mean, and the dark blue vertical dashed line marks the three sigma value. The TMF peak value is indicated in red. The total amount of points, the 97th quantile and the percentage of total momentum flux associated with values larger than the quantile are indicated in the upper right corner of each plot (see text for details). The plots were made using the 4 hr, 4 km total momentum flux estimates averaged between 86 and 93 km of altitude.

positive at all altitudes for almost the entire season. On the other hand, during the winter,  $\langle u'w' \rangle$  changes from negative to positive values at approximately the same altitude range in which the mean zonal wind reverses direction from eastward to westward. In summertime,  $\langle u'w' \rangle$  over SIMONe Argentina is characterized by positive values dominating below  $\sim 90$  km until the end of January, a time period when strong westward mean zonal winds prevail at these altitudes (e.g., Iimura et al., 2011). In the case of MMARIA-SAAMER, the positive values observed below 90 km of altitude are weaker and disappear prematurely. Despite the dominance of strong westward mean zonal winds until the end of February,  $\langle u'w' \rangle$  becomes negative already at the beginning of January, a couple of weeks earlier than what the climatology of  $\langle u'w' \rangle$  at Tierra del Fuego shows (e.g., de Wit et al., 2017).

Although not shown here, it is worth mentioning that the 28-day mean momentum fluxes have statistical uncertainties in the order of 10%–15%, for the height range considered in this work. The propagated errors, on the other hand, are approximately one order of magnitude smaller than the statistical uncertainties (for more details, see Conte et al. (2021)).

### 4.3. Intermittency in the Total Momentum Flux

In this section, the focus is set on the short-term variability of the momentum fluxes. Particularly, results on the intermittency in the total momentum flux (TMF) are presented. The TMF ( $\text{m}^2/\text{s}^2$ ), or equivalently the Reynolds stress normalized by the air density ( $\tau_R/\rho$ ), is defined as

$$TMF = \sqrt{\langle u'w' \rangle^2 + \langle v'w' \rangle^2}. \quad (3)$$

The TMF values were calculated using the 4 hr, 4 km momentum fluxes described in Section 3. To assess the intermittency in the TMF, Figure 6 shows the logarithmic distributions of the 4 hr, 4 km total momentum fluxes averaged between 86 and 93 km of altitude, for the period 1 December 2019–31 March 2020. From left to right and top to bottom, the plots correspond to SIMONe Peru, CONDOR, SIMONe Argentina and MMARIA-SAAMER.



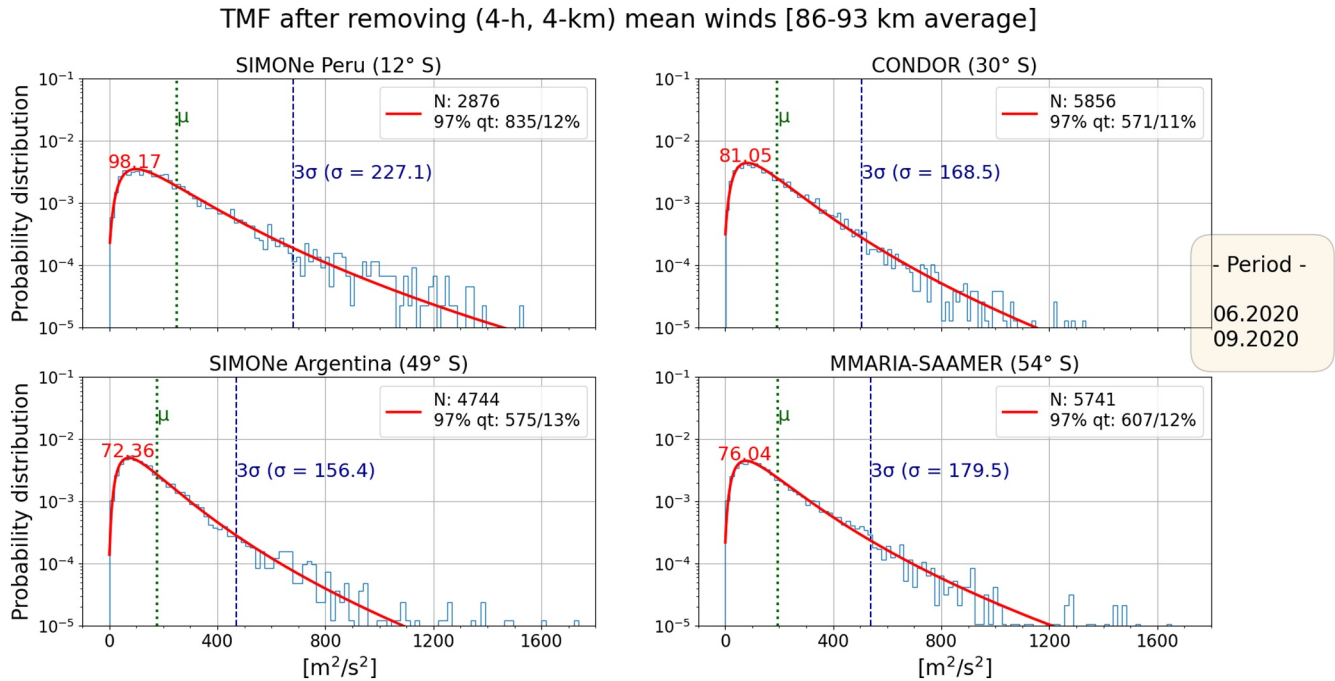


**Figure 7.** Same as Figure 6, but during the southern hemisphere winter season.

Figure 7 shows analogous plots, but for the period 1 June 2020–30 September 2020. In both figures, the observed distributions were fitted with a log-normal function

$$\frac{1}{x\mu\sqrt{2\pi}}\exp\left(-\frac{\log^2(x)}{2\sigma^2}\right), \quad (4)$$

where  $x$  are the TMF values averaged between 86 and 93 km of height. Initial values equal to the mean and the standard deviation were given to  $\mu$  and  $\sigma$ , respectively. An iterative process was then implemented to find the curve that best fits the data. Only one iteration was required to find the best fit. This curve is indicated in red, and its corresponding values for  $\mu$  and  $3\sigma$  are indicated with the vertical green dotted and blue dashed lines, respectively.

A quick inspection of Figures 6 and 7 reveals that the log-normal function fits well the TMF distributions at the four locations, for both the summer and winter seasons. In the summer, the fitted curves have similar shapes between SIMONE Peru and CONDOR, and between SIMONE Argentina and MMARIA-SAAMER. However, their shape is wider over SIMONE Peru and CONDOR, compared to SIMONE Argentina and MMARIA-SAAMER. During the winter, the fitted log-normal functions have similar shapes at CONDOR and the two systems located in southern Patagonia. The log-normal function for SIMONE Peru differs slightly from the other three due to less statistics as a result of the almost 2 months of missing data. Compared to summer, the peak values of the distributions are larger during the winter at the four locations.

To assess the contribution of large momentum fluxes to the total flux, 97th quantiles, and the percentage of total momentum flux estimates associated with values larger than the quantiles are indicated in the upper right corners of the plots presented in Figures 6 and 7. These values were calculated following Hertzog et al. (2012), that is, by computing

$$100 \times \frac{\sum_{tmf_j > tmf_r} (tmf)_j}{\sum_{i=1}^N (tmf)_i}. \quad (5)$$

Here,  $N$  is the total amount of total momentum flux estimates,  $tmf_j$  is the  $j$ th TMF estimate, and  $tmf_r$  verifies that  $\sum_{tmf_j > tmf_r} (j) = N(1 - r)$ . For the 97th quantile,  $r$  is equal to 0.97.

Notice that despite the fact that during the summer the 97th quantiles are about 40% larger over SIMONe Peru and CONDOR, the percentage of TMFs greater than the quantiles is similar at the four locations, with values in the order of 12%. In wintertime, the 97th quantiles are larger over SIMONe Argentina and MMARIA-SAAMER, but similar percentage values of around 12% are obtained at all the locations.

## 5. Discussion

Our results on mean winds and tides were presented to provide context for the discussion of the momentum fluxes. Besides, the main characteristics of the mean winds and tides at most of the locations explored in this work have already been discussed in previous literature (e.g., Chau et al., 2021; Conte et al., 2017, 2021; Fritts et al., 2012; He et al., 2021). For these reasons, the discussion is focused on the 28-day mean momentum fluxes and the distributions of the 4 hr, 4 km total momentum fluxes, and only one comment is made here regarding the mean winds. It can be noticed that there is an altitude gap of approximately 15 km between the MERRA-2 and the multistatic SMR mean horizontal winds. This is a shortcoming of our approach. However, since the mean winds have been explored in a monthly basis (28-day basis, to be precise), one shouldn't expect significant changes in the mean horizontal winds between 65 and 80 km of altitude, specially when no sudden stratospheric warmings occurred during the time periods investigated in this study.

### 5.1. 28-Day Mean Momentum Fluxes

The differences observed in the 28-day mean momentum fluxes between SIMONe Peru and CONDOR may be partly explained as a consequence of distinct filtering effects of the mean winds and tides. From Figures 2 and 3, it can be seen that above ~30 km of altitude the mean zonal and meridional winds are quite different between SIMONe Peru and CONDOR, during both summer and winter seasons. Clearly, different background flow conditions will have distinct impacts on the propagation, dissipation and breaking of GWs (e.g., Holton, 2004). For example, notice that during winter, between ~86 and 95 km of altitude over CONDOR, although the mean zonal wind reverses from eastward to westward,  $\langle u'w' \rangle$  remains intriguingly positive. In turn, over SIMONe Peru, during the second half of the winter,  $\langle u'w' \rangle$  is positive at the same altitudes where the mean zonal wind is westward directed. In the case of SIMONe Argentina and MMARIA-SAAMER, the mean winds and tides behave very similarly. This suggests that the differences observed in the mean momentum fluxes between these two systems are mostly due to distinct GW characteristics, for example, different sources triggering the waves. For example, notice that during the winter below ~90 km of altitude,  $\langle v'w' \rangle$  is poleward at SIMONe Argentina, but equatorward at MMARIA-SAAMER. This may indicate that GWs break at different altitudes not because of different background conditions, but due to different intrinsic characteristics of the waves. In other words, our results show that in southern Patagonia, the differences in the MLT mean momentum flux dynamics between 49°S and 54°S are coupled to source variability in the lower stratosphere and troposphere regions. At Tierra del Fuego, the connection to variability in the stratosphere has already been suggested by de Wit et al. (2017). They speculated that the momentum flux over SAAMER may be mostly dominated by secondary GWs resulting from large mountain waves breaking at stratospheric altitudes.

The waves driving the momentum flux estimates here discussed have horizontal scales in the order of 400 km or less. This implies that the momentum fluxes presented in Figures 4 and 5 are mostly dominated by primary GWs and/or non-primary GWs. The latter term refers to secondary GWs generated by nonlinear processes. In such cases, the primary wave breaks and cascades into smaller scales (e.g., Andreassen et al., 1994; Dörnbrack, 1998; Fritts et al., 2009). The wave breaking produces localized forcing, which in turn triggers new waves with scales that are smaller than those of the primary wave (e.g., Chun & Kim, 2008; Heale et al., 2020). On the other hand, linear secondary GWs result from dissipation of the primary waves into single wave packets. Linear secondary GWs have horizontal scales in the order of a thousand km or more (e.g., Vadas et al., 2003; Vadas et al., 2018). If the latter type of waves were the main drivers of the momentum fluxes over, for example, SIMONe Argentina and MMARIA-SAAMER, then similar characteristics should be observed in the wave dynamics at these two locations, at least on average. However, Figures 4 and 5 show clear differences in both the zonal and meridional momentum fluxes over these two systems, which indicates that only waves with horizontal scales of a few hundred km or less are present. This was expected, since the effects of large-scale GWs are (mostly) removed after subtracting the 4 hr, 4 km mean horizontal winds. Note that this does not imply that linear secondary GWs are not

present in the MLT over the locations here studied. It only means that their effects are removed by the estimation procedure applied to the SMR data.

From our analysis, it is not possible to determine if primary or non-primary gravity waves dominate the momentum flux dynamics at MLT altitudes over the regions here explored. Nonetheless, given the strong winds that blow over the Andes mountain range in southern Patagonia (e.g., Eckermann & Preusse, 1999; Rapp et al., 2020), we are more inclined to favor the orography as the main source of the primary GWs that drive the momentum fluxes over SIMONe Argentina and MMARIA-SAAMER. In fact, previous studies have already shown that the middle atmosphere over these parts of Patagonia is significantly influenced by strong mountain wave events (e.g., de Wit et al., 2017; Fritts et al., 2021; Lund et al., 2020, and references therein). On the other hand, non-orographic sources such as spontaneous emission from jets and convection should be taken into consideration as well. For example, waves from the stratospheric GW belt that develops at middle latitudes of the southern hemisphere during winter (e.g., Hendricks et al., 2014), may propagate higher up and deposit their momentum at MLT altitudes.

A similar reasoning can be applied in the case of CONDOR. Gravity waves generated by deep convection over the northeast of Argentina, for example, may be trapped in ducts and travel to higher latitudes where then they deposit their momentum (e.g., Hecht et al., 2001; Simkhada et al., 2009). Besides, secondary GWs resulting from breaking of primary waves generated by deep convection have also been reported at MLT altitudes over CONDOR (e.g., Vargas et al., 2016). On the other hand, orographic GWs are also expected to occur given the presence of high mountains (e.g., Hecht et al., 2018). In the case of SIMONe Peru, it is more likely that convective GWs play the dominant role, since deep convection is a prolific generator of GWs at low latitudes (e.g., Walterscheid & Christensen, 2016).

The large amplitudes observed in the momentum flux estimates are intriguing. We think they result from the following factors: (a) that the wave activity over the Andes mountain range is indeed very strong, as it has been reported by some previous studies (e.g., de Wit et al., 2017; Trinh et al., 2018). (b) That  $\langle u'w' \rangle$  and  $\langle v'w' \rangle$  are equivalent to the zero-lag second order statistics of the wind velocities introduced by Vierinen et al. (2019). This means that  $\langle u'w' \rangle$  and  $\langle v'w' \rangle$  are overestimates of the actual values since they are affected by the correlated errors. (c) An overestimation of the momentum fluxes inherent to SMR systems. Charuvil Asokan et al. (2021) have demonstrated that unresolved small-scale (less than 400–500 km) horizontal variability leaks into the vertical direction. They showed that this leakage affects SMR observations by increasing 1–2 m/s the amplitude of the estimated vertical velocities. This so-called contamination from the small-scale horizontal variability adversely affects the  $\langle u'w' \rangle$  and  $\langle v'w' \rangle$  estimates as well. Our preliminary assessments indicate that this overestimation is in the order of at least 10%–20% (not shown here). It is for this reason that we are currently working on the validation of SMR based momentum flux estimates using high resolution forward model data, similarly to what has been done in Charuvil Asokan et al. (2021).

## 5.2. Intermittency in the 4-hr, 4-km Total Momentum Flux

Intermittency in atmospheric flows can be identified by the non-Gaussian form of the probability density function (PDF) of the wind, for example. The higher the intermittency, the further the distribution of the observed geophysical parameter is from a Gaussian form (e.g., Pouquet, 2018). In other words, intermittency is a consequence of multiplicative processes. In Figures 6 and 7 it is shown that the PDFs are wider over SIMONe Peru and CONDOR, compared to SIMONe Argentina and MMARIA-SAAMER. A wider PDF is not only an indicator of stronger intermittency (e.g., Ern et al., 2021), but it also shows that there are more GWs with larger amplitudes over SIMONe Peru and CONDOR, where the TMF peak values are near 70 m<sup>2</sup>/s<sup>2</sup>. In the case of SIMONe Argentina and MMARIA-SAAMER, the PDFs have peak values of ~47 m<sup>2</sup>/s<sup>2</sup>. During the winter, similar features can be identified when comparing the PDFs obtained for the different systems. However, the TMF over the four locations presents wider PDFs and larger peak values than during the summer. This is partly due to the fact that MLT winds are more variable during the winter (e.g., Hoffmann et al., 2010; Vincent, 2015).

GW intermittency arises from the random nature of the sources triggering the primary waves, from the changes experienced by the medium in which these waves propagate, that is, by changes in the background wind, or from both (e.g., Cao & Liu, 2016; Wright et al., 2013). Usually, the former is understood as the main cause of GW intermittency at stratospheric altitudes, that is, at altitudes closer to the primary GW sources. However, in the MLT region, the intermittency may be most likely the result of changes in the background flow. GW intermittency due



to wind variability has already been reported at high latitudes in the southern hemisphere (e.g., Love & Murphy, 2016). Besides, generation of secondary GWs and stratified turbulence have also been identified as sources of intermittency at MLT altitudes (e.g., Avsarkisov, 2020; Vadas & Becker, 2018). Satellite studies have shown that the PDFs of the TMF have longer tails over mountain areas, and that they tend to be skewed toward low values at low latitudes (e.g., Ern et al., 2021). Our results show the opposite, with longer tails observed at middle to low latitude locations, and summertime PDFs more skewed to smaller values over SIMONE Argentina and MMARIA-SAAMER. However, the four locations analyzed in our study correspond to different sectors above the Andes, where mountain wave events contribute significantly to the momentum flux, particularly during the winter, and hence widen the shape of the PDFs. Besides, TMF estimates based on satellite measurements capture the effects of waves with horizontal scales larger than ~600 km, while our momentum fluxes correspond to irregularities with horizontal scales of 400 km or less.

Our results on the TMF 97th quantiles show that at four different sectors over the Andes mountain range, the contributions from large momentum fluxes are very similar during both summer and winter seasons (around 12%). On the other hand, the shape of the PDFs around small values during summer is different between SIMONE Peru/CONDOR and SIMONE Argentina/MMARIA-SAAMER. In the winter, differences in the shape of the PDFs around small values are not evident. This suggests that the activity of small GWs at MLT altitudes during summer is not the same over the entire Andes mountain range, but it can be similar during winter months. Global circulation models may benefit from these results, by implementing non-homogeneous (homogeneous) GW drag schemes during summer (winter) over the South American Andean region.

## 6. Concluding Remarks

Mesosphere and lower thermosphere momentum fluxes obtained from measurements provided by four multistatic SMR networks located at different sectors near the Andes mountain range have been presented and compared for the first time. Our results show that MLT GW-driven momentum fluxes vary significantly depending on the location and the season; and that this variability is not the same for large and small amplitude GWs. Zonal and meridional momentum fluxes,  $\langle u'w' \rangle$  and  $\langle v'w' \rangle$ , respectively, were estimated after subtracting 4 hr, 4 km mean horizontal winds, for altitudes between 80 and 99 km. For this purpose, Doppler shift measurements provided by SIMONE Peru (12°S; spread spectrum system), CONDOR (30°S; pulsed system), SIMONE Argentina (49°S; spread spectrum system) and MMARIA-SAAMER (54°S; pulsed system) were considered. Comparison analyses were made not only among the four systems, but also between two different periods: 1 December 2019–31 March 2020 (southern hemisphere summer season), and 1 June 2020–30 September 2020 (southern hemisphere winter season).

First, 28-day mean values of  $\langle u'w' \rangle$  and  $\langle v'w' \rangle$  were calculated. This was done for two reasons: (a) To reduce the momentum flux statistical uncertainties to values in the order of 10%–15%; and (b) to explore the differences in the mean momentum deposited by waves with horizontal scales of less than ~400 km. Our main findings are: (a) The mean wave dynamics are different among the four locations, and between the summer and winter times. (b) At low to middle latitudes (SIMONE Peru and CONDOR), the 28-day  $\langle u'w' \rangle$  and  $\langle v'w' \rangle$  are stronger than over the region of southern Patagonia (SIMONE Argentina and MMARIA-SAAMER). (c)  $\langle v'w' \rangle$  has larger amplitudes than  $\langle u'w' \rangle$  at the four locations, during both summer and winter seasons. (d) The differences in the momentum fluxes between SIMONE Peru and CONDOR can be partly attributed to distinct filtering effects of the mean winds and dominant tides. (e) Mean winds and tides behave very similarly over SIMONE Argentina and MMARIA-SAAMER, which suggests that the observed differences in  $\langle u'w' \rangle$  and  $\langle v'w' \rangle$  are due to differences in the GW sources. (f) Effects of linear secondary GWs are mostly removed by the procedure applied to the SMR data to extract information on  $\langle u'w' \rangle$  and  $\langle v'w' \rangle$ . For this reason, primary and/or non-primary GWs are the main drivers of the momentum fluxes presented in this study. Although it was briefly discussed in Section 5, determining the types of waves that dominate the observed momentum fluxes, and at which locations they do so, is left for future studies.

Finally, preliminary results on the intermittency of the total momentum flux were presented. At the four locations, log-normal probability density functions represent very well the seasonal distributions of the 4 hr, 4 km total momentum fluxes averaged between 86 and 93 km of altitude. During the summer, the shapes of the PDFs are wider at low to middle latitudes (12° S and 30°S), compared to middle latitudes (49°S and 54°S). In the winter,

the shape of the PDF is similar at the four locations, although wider than in summer. The latter indicates that the TMF intermittency is higher during the winter, in agreement with previous studies. The percentages of total momentum fluxes greater than the 97th quantiles are around 12% for both seasons at the four sites. This indicates that the contributions from large momentum fluxes to the total flux are almost the same at the four locations during both the aestival and wintry periods.

## Data Availability Statement

The specular meteor radar data products used to produce the figures presented in this article can be found in HDF5 format at <https://doi.org/10.22000/501>. Modern-Era Retrospective analysis for Research and Applications, Version 2 (MERRA-2) data can be accessed at [https://disc.gsfc.nasa.gov/datasets/M2I3NPASM\\_5.12.4/summary](https://disc.gsfc.nasa.gov/datasets/M2I3NPASM_5.12.4/summary).

## Acknowledgments

We thank Nico Pfeffer, Nahuel Díaz, Facundo Olivares, Martín “el griego” Palopoli, and Pablo Quiroz for their constant support and help in maintaining SIMONe Argentina sites. We thank Karim Kuyeng for supporting operations of SIMONe Peru. The CONDOR meteor radar system in Chile is funded by the National Science Foundation through grant AGS-1828 589. The system was built and deployed by ATRAD Ltd. A. Liu acknowledges the excellent support provided by The Association of Universities for Research in Astronomy (AURA), Las Campanas Observatory (LCO), and Southern Cross (Cruz del Sur) Observatory for the deployment and operation of this radar system. We thank the staff at Estación Astronómica Río Grande for supporting the operations of SAAMER and MMARIA-SAAMER. SAAMER's operation is supported by NASA NESAC assessment TI-17-01 204. We thank Diego Janches for valuable input regarding SAAMER. The work of J.F.Conte is supported by the Bundesministerium für Bildung und Forschung via project WASCLIM-IAP part of the ROMIC-II program. Open access funding enabled and organized by Projekt DEAL.

## References

- Andreassen, Ø., Wasberg, C. E., Fritts, D. C., & Isler, J. R. (1994). Gravity wave breaking in two and three dimensions, 1, model description and comparison of two-dimensional evolutions. *Journal of Geophysical Research*, 99, 8095–8108. <https://doi.org/10.1029/93jd03435>
- Andrews, D. G., Holton, J. R., & Leovy, C. B. (1987). *Middle atmosphere dynamics* (pp. 421–422). Academic Press. <https://doi.org/10.1002/qj.49711548612>
- Andrioli, V. F., Fritts, D. C., Batista, P. P., & Clemesha, B. R. (2013). Improved analysis of all-sky meteor radar measurements of gravity wave variances and momentum fluxes. *Annals of Geophysics*, 31, 889–908. <https://doi.org/10.5194/angeo-31-889-2013>
- Avsarkisov, V. (2020). On the buoyancy subrange in stratified turbulence. *Atmosphere*, 11, 659. <https://doi.org/10.3390/atmos11060659>
- Cao, B., & Liu, A. Z. (2016). Intermittency of gravity wave momentum flux in the mesopause region observed with an all-sky airglow imager. *Journal of Geophysical Research*, 121, 650–663. <https://doi.org/10.1002/2015JD023802>
- Charuvil Asokan, H., Chau, J. L., Larsen, M. F., Conte, J. F., Marino, R., Vierinen, J., et al. (2021). Validation of multistatic meteor radar analysis using modeled mesospheric dynamics: An assessment of the reliability of gradients and vertical velocities. *Journal of Geophysical Research*
- Chau, J. L., & Clahsen, M. (2019). Empirical phase calibration for multi-static specular meteor radars using a beam-forming approach and arbitrary interferometric configurations. *Radio Science*, 54, 60–71. <https://doi.org/10.1029/2018RS006741>
- Chau, J. L., Urco, J. M., Vierinen, J., Harding, B. J., Clahsen, M., Pfeffer, N., et al. (2021). Multistatic specular meteor radar network in Peru: System description and initial results. *Earth and Space Science*, 8(1). <https://doi.org/10.1029/2020EA001293>
- Chun, H., & Kim, Y. H. (2008). Secondary waves generated by breaking of convective gravity waves in the mesosphere and their influence in the wave momentum flux. *Journal of Geophysical Research*, 113, D23107. <https://doi.org/10.1029/2008JD009792>
- Conte, J. F., Chau, J. L., Laskar, F. I., Stober, G., Schmidt, H., & Brown, P. (2018). Semidiurnal solar tide differences between fall and spring transition times in the northern hemisphere. *Annales Geophysicae*, 36, 999–1008. <https://doi.org/10.5194/angeo-36-999-2018>
- Conte, J. F., Chau, J. L., & Peters, D. H. W. (2019). Middle- and high-latitude mesosphere and lower thermosphere mean winds and tides in response to strong polar-night jet oscillations. *Journal of Geophysical Research: Atmospheres*, 124, 9262–9276. <https://doi.org/10.1029/2019JD030828>
- Conte, J. F., Chau, J. L., Stober, G., Pedatella, N., Maute, A., Hoffmann, P., et al. (2017). Climatology of semidiurnal lunar and solar tides at middle and high latitudes: Interhemispheric comparison. *Journal of Geophysical Research: Space Physics*, 122, 7750–7760. <https://doi.org/10.1002/2017JA024396>
- Conte, J. F., Chau, J. L., Urco, J. M., Latteck, R., Vierinen, J., & Salvador, J. O. (2021). First studies of mesosphere and lower thermosphere dynamics using a multistatic specular meteor radar network over southern Patagonia. *Earth and Space Science*, 8, e2020EA001356. <https://doi.org/10.1029/2020EA001356>
- de Wit, R. J., Janches, D., Fritts, D. C., & Hibbins, R. E. (2016). QBO modulation of the mesopause gravity wave momentum flux over Tierra del Fuego. *Geophysical Research Letters*, 43, 4049–4055. <https://doi.org/10.1002/2016GL068599>
- de Wit, R. J., Janches, D., Fritts, D. C., Stockwell, R. G., & Coy, L. (2017). Unexpected climatological behavior of MLT gravity wave momentum flux in the lee of the southern Andes hot spot. *Geophysical Research Letters*, 44, 1182–1191. <https://doi.org/10.1002/2016GL072311>
- Dörnbrack, A. (1998). Turbulent mixing by breaking gravity waves. *Journal of Fluid Mechanics*, 375, 113–141. <https://doi.org/10.1017/S0022112098002833>
- Eckermann, S. D., & Preusse, P. (1999). Global measurements of stratospheric mountain waves from space. *Science*, 286, 1534–1537. <https://doi.org/10.1126/science.286.5444.1534>
- Ern, M., Diallo, M., Preusse, P., Mlynarczyk, M. G., Schwartz, M. J., Wu, Q., & Riese, M. (2021). The semiannual oscillation (sao) in the tropical middle atmosphere and its gravity wave driving in reanalyses and satellite observations. *Atmospheric Chemistry and Physics*, 21(18). <https://doi.org/10.5194/acp-2021-190>
- Ern, M., Preusse, P., Alexander, M. J., & Warner, C. D. (2004). Absolute values of gravity wave momentum flux derived from satellite data. *Journal of Geophysical Research*, 109, D20103. <https://doi.org/10.1029/2004JD004752>
- Fritts, D. C., & Alexander, M. J. (2003). Gravity wave dynamics and effects in the middle atmosphere. *Reviews of Geophysics*, 41(1). <https://doi.org/10.1029/2001RG000106>
- Fritts, D. C., Janches, D., & Hocking, W. K. (2010). Southern Argentina Agile meteor radar: Initial assessment of gravity wave momentum fluxes. *Journal of Geophysical Research*, 115. <https://doi.org/10.1029/2010JD013891>
- Fritts, D. C., Janches, D., Hocking, W. K., Mitchell, N. J., & Taylor, M. J. (2012). Assessment of gravity wave momentum flux measurement capabilities by meteor radars having different transmitter power and antenna configurations. *Journal of Geophysical Research*, 117, D10108. <https://doi.org/10.1029/2011JD017174>
- Fritts, D. C., Janches, D., Iimura, H., Hocking, W. K., Mitchell, N. J., Stockwell, R. G., et al. (2010). Southern Argentina Agile meteor radar: System design and initial measurements of large-scale winds and tides. *Journal of Geophysical Research*, 115(D18). <https://doi.org/10.1029/2010JD013850>
- Fritts, D. C., Lund, T. S., Wan, K., & Liu, H.-L. (2021). Numerical simulation of mountain waves over the southern Andes, part 2: Momentum fluxes and wave/mean-flow interactions. *Journal of the Atmospheric Sciences*, 78, 3069–3088. <https://doi.org/10.1175/JAS-D-20-0207.1>

- Fritts, D. C., Wang, L., Werne, J., Lund, T., & Wan, K. (2009). Gravity wave instability and dynamics at high Reynolds numbers. Part I: Wave field evolution at large amplitudes and high frequencies. *Journal of the Atmospheric Sciences*, 66, 1126–1148. <https://doi.org/10.1175/2008jas2726.1>
- Garcia, R. R., & Boville, B. A. (1994). Downward control of the mean meridional circulation and temperature distribution of the polar winter stratosphere. *Journal of the Atmospheric Sciences*, 51(15), 2238–2245. [https://doi.org/10.1175/1520-0469\(1994\)051<2238:cotmmc>2.0.co;2](https://doi.org/10.1175/1520-0469(1994)051<2238:cotmmc>2.0.co;2)
- Geldenhuis, M., Preusse, P., Krisch, I., Zülicke, C., Ungermann, J., Ern, F., et al. (2021). Orographically-induced spontaneous imbalance within the jet causing a large scale gravity wave event. *Atmospheric Chemistry and Physics*, 21, 10393–10412. <https://doi.org/10.5194/acp-21-10393-2021>
- He, M., Chau, J. L., Forbes, J. M., Zhang, X., Englert, C. R., Harding, B. J., et al. (2021). Quasi-2-day wave in low-latitude atmospheric winds as viewed from the ground and space during January–March, 2020. *Geophysical Research Letters*, 48, e2021GL093466. <https://doi.org/10.1029/2021GL093466>
- Heale, C. J., Bossert, K., Vadas, S. L., Hoffmann, L., Dörnbrack, A., Stober, G., et al. (2020). Secondary gravity waves generated by breaking mountain waves over Europe. *Journal of Geophysical Research: Atmospheres*, 125, e2019JD031662. <https://doi.org/10.1029/2019JD031662>
- Hecht, J. H., Fritts, D. C., Wang, L., Gelinas, L. J., Rudy, R. J., Walterscheid, R. L., et al. (2018). Observations of the breakdown of mountain waves over the Andes Lidar observatory at Cerro Pachon on 8/9 July 2012. *Journal of Geophysical Research: Atmospheres*, 123, 276–299. <https://doi.org/10.1002/2017JD027303>
- Hecht, J. H., Walterscheid, R. L., Hickey, M. P., & Franke, S. J. (2001). Climatology and modeling of quasi-monochromatic gravity waves observed over Urbana Illinois. *Journal of Geophysical Research*, 106, 5181–5195. <https://doi.org/10.1029/2000JD900722>
- Hendricks, E. A., Doyle, J. D., Eckermann, S. D., Jiang, Q., & Reinecke, P. A. (2014). What is the source of the stratospheric gravity wave belt in austral winter? *Science*, 343(6158), 1583–1592. <https://doi.org/10.1126/science.1253332>
- Hertzog, A., Alexander, M. J., & Plougonven, R. (2012). On the intermittency of gravity wave momentum flux in the stratosphere. *Journal of the Atmospheric Sciences*, 69, 3433–3448. <https://doi.org/10.1175/JAS-D-12-09.1>
- Hocking, W. K. (2005). A new approach to momentum flux determinations using SKiYMET meteor radars. *Annales Geophysicae*, 23(7), 2433–2439. <https://doi.org/10.5194/angeo-23-2433-2005>
- Hoffmann, P., Becker, E., Singer, W., & Placke, M. (2010). Seasonal variation of mesospheric waves at northern middle and high latitudes. *Journal of Atmospheric and Solar-Terrestrial Physics*, 72(14–15), 1068–1079. <https://doi.org/10.1016/j.jastp.2010.07.002>
- Holton, J. R. (2004). *An introduction to dynamic meteorology* (4th ed.). Elsevier Academic Press.
- Imura, H., Fritts, D. C., Tsutsumi, M., Nakamura, T., Hoffmann, P., & Singer, W. (2011). Long-term observations of the wind field in the Antarctic and Arctic mesosphere and lower-thermosphere at conjugate latitudes. *Journal of Geophysical Research*, 116, D20112. <https://doi.org/10.1029/2011JD016003>
- Janches, D., Close, S., Hormaechea, J. L., Swarnalingam, N., Murphy, A., O'Connor, D., et al. (2015). The southern Argentina Agile meteor radar orbital system (SAAMER-OS): An initial sporadic meteoroid orbital survey in the southern sky. *The Astrophysical Journal*, 809(1), 36. <https://doi.org/10.1088/0004-637X/809/1/36>
- Kudeki, E., & Franke, S. J. (1998). Statistics of momentum flux estimation. *Journal of Atmospheric and Solar-Terrestrial Physics*, 60, 1549–1553. [https://doi.org/10.1016/S1364-6826\(98\)00104-7](https://doi.org/10.1016/S1364-6826(98)00104-7)
- Love, P. T., & Murphy, D. J. (2016). Gravity wave momentum flux in the mesosphere measured by VHF radar at Davis, Antarctica. *Journal of Geophysical Research: Atmospheres*, 121, 12723–12812. <https://doi.org/10.1002/2016JD025627>
- Lund, T., Fritts, D., Kam, W., Laughman, B., & Liu, H.-L. (2020). Numerical simulation of mountain waves over the southern Andes, Part 1: Mountain wave and secondary wave character, evolutions, and breaking. *Journal of the Atmospheric Sciences*, 77(12), 4337–4356. <https://doi.org/10.1175/JAS-D-19-0356.1>
- Morgenstern, O., Giorgetta, M. A., Shibata, K., Eyring, V., Waugh, D. W., Shepherd, T. G., et al. (2010). Review of the formulation of present-generation stratospheric chemistry-climate models and associated external forcings. *Journal of Geophysical Research*, 115, D00M02. <https://doi.org/10.1029/2009JD013728>
- Oberheide, J., Forbes, J. M., Häusler, K., Wu, Q., & Bruinsma, S. L. (2009). Tropospheric tides from 80 to 400 km: Propagation, interannual variability, and solar cycle effects. *Journal of Geophysical Research*, 114, D00I05. <https://doi.org/10.1029/2009JD012388>
- Pancheva, D., & Mukhtarov, P. (2011). Atmospheric tides and planetary waves: Recent progress based on SABER/TIMED temperature measurements (2002–2007). *Aeronomy of the Earth's Atmosphere and Ionosphere, IAGA Special Sopron Book Series 2*. <https://doi.org/10.1007/978-94-007-0326-12>
- Placke, M., Hoffmann, P., Becker, E., Jacobi, C., Singer, W., & Rapp, M. (2011b). Gravity wave momentum fluxes in the MLT—Part II: Meteor radar investigations at high and midlatitudes in comparison with modeling studies. *Journal of Atmospheric and Solar-Terrestrial Physics*, 73, 911–920. <https://doi.org/10.1016/j.jastp.2010.05.007>
- Pouquet, A. (2018). Intermittent turbulence in a global ocean model. *Physics*, 11(21). <https://doi.org/10.1103/Physics.11.21>
- Preusse, P., Dörnbrack, A., Eckermann, S. D., Riese, M., Schaeler, B., Bacmeister, J. T., et al. (2002). Space-based measurements of stratospheric mountain waves by CRISTA: 1. Sensitivity, analysis method, and a case study. *Journal of Geophysical Research*, 107(D23). <https://doi.org/10.1029/2001JD000699>
- Rapp, M., Kaifler, B., Dörnbrack, A., Gisinger, S., Mixa, T., Reichert, R., et al. (2020). SOUTHTRAC-GW: An airborne field campaign to explore gravity wave dynamics at the world's strongest hotspot. *Bulletin of the American Meteorological Society*, 1–60. <https://doi.org/10.1175/BAMS-D-20-0034.1>
- Sandford, D. J., Muller, H. G., & Mitchell, N. J. (2006). Observations of lunar tides in the mesosphere and lower thermosphere at Arctic and middle latitudes. *Atmospheric Chemistry and Physics*, 6, 4117–4127. <https://doi.org/10.5194/acp-6-4117-2006>
- Sato, K., & Dunkerton, T. J. (1997). Estimates of momentum flux associated with equatorial kelvin and gravity waves. *Journal of Geophysical Research*, 102(D22), 26247–26261. <https://doi.org/10.1029/96JD02514>
- Simkhada, D. B., Snively, J. B., Taylor, M. J., & Franke, S. J. (2009). Analysis and modeling of ducted and evanescent gravity waves observed in the Hawaiian airglow. *Annals of Geophysics*, 27, 3213–3224. <https://doi.org/10.5194/angeo-27-3213-2009>
- Spargo, A. J., Reid, I. M., & MacKinnon, A. D. (2019). Multistatic meteor radar observations of gravity-wave–tidal interaction over southern Australia. *Atmospheric Measurement Techniques*, 12, 4791–4812. <https://doi.org/10.5194/amt-12-4791-2019>
- Stening, R. J., Forbes, J. M., Hagan, M. E., & Richmond, A. D. (1997). Experiments with a lunar atmospheric tidal model. *Journal of Geophysical Research*, 102, 13465–13471. <https://doi.org/10.1029/97JD00778>
- Stephan, C. C., Strube, C., Klocke, D., Ern, M., Hoffmann, L., Preusse, P., & Schmidt, H. (2019). Gravity waves in global high-resolution simulations with explicit and parameterized convection. *Journal of Geophysical Research: Atmospheres*, 124(8), 4446–4459. <https://doi.org/10.1029/2018JD030073>
- Stober, G., & Chau, J. L. (2015). A multistatic and multifrequency novel approach for specular meteor radars to improve wind measurements in the MLT region. *Radio Science*, 50, 431–442. <https://doi.org/10.1002/2014RS005591>



- Stober, G., Chau, J. L., Vierinen, J., Jacobi, C., & Wilhelm, S. (2018). Retrieving horizontally resolved wind fields using multi-static meteor radar observations. *Atmospheric Measurement Techniques*, 11, 4891–4907. <https://doi.org/10.5194/amt-11-4891-2018>
- Stober, G., Janches, D., Matthias, V., Fritts, D., Marino, J., Moffat-Griffin, T., et al. (2021). Seasonal evolution of winds, atmospheric tides, and Reynolds stress components in the southern hemisphere mesosphere–lower thermosphere in 2019. *Annals of Geophysics*, 39, 1–29. <https://doi.org/10.5194/angeo-39-1-2021>
- Thorsen, D., Franke, S. J., & Kudeki, E. (1997). A new approach to MF radar interferometry for estimating mean winds and momentum flux. *Radio Science*, 32(2), 707–726. <https://doi.org/10.1029/96rs03422>
- Trinh, Q. T., Ern, M., Doornbos, E., Preusse, P., & Riese, M. (2018). Characteristics of the quiet-time hot spot gravity waves observed by GOCE over the Southern Andes on 5 July 2010. *Annals of Geophysics*, 36, 425–444. <https://doi.org/10.5194/angeo-36-425-2018>
- Urco, J. M., Chau, J. L., Weber, T., & Latteck, R. (2019). Enhancing the spatio-temporal features of polar mesosphere Summer echoes using coherent MIMO and radar imaging at MAARSY. *Atmospheric Measurement Techniques*, 12, 955–969. <https://doi.org/10.5194/amt-12-955-2019>
- Vadas, S. L., & Becker, E. (2018). Numerical modeling of the excitation, propagation, and dissipation of primary and secondary gravity waves during wintertime at McMurdo station in the Antarctic. *Journal of Geophysical Research: Atmospheres*, 123(17), 9326–9369. <https://doi.org/10.1029/2017JD027974>
- Vadas, S. L., Fritts, D. C., & Alexander, M. J. (2003). Mechanism for the generation of secondary waves in wave breaking regions. *Journal of the Atmospheric Sciences*, 60, 194–214. [https://doi.org/10.1175/1520-0469\(2003\)060<0194:mftgos>2.0.co;2](https://doi.org/10.1175/1520-0469(2003)060<0194:mftgos>2.0.co;2)
- Vadas, S. L., Zhao, J., Chu, X., & Becker, E. (2018). The excitation of secondary gravity waves from local body forces: Theory and observation. *Journal of Geophysical Research: Atmospheres*, 123, 9296–9369. <https://doi.org/10.1029/2017JD027974>
- Vargas, F., Swenson, G., Liu, A., & Pautet, D. (2016). Evidence of the excitation of a ring-like gravity wave in the mesosphere over the Andes Lidar observatory. *Journal of Geophysical Research: Atmospheres*, 121, 8896–8912. <https://doi.org/10.1002/2016JD024799>
- Vierinen, J., Chau, J. L., Charuvil, H., Urco, J. M., Clahsen, M., Avsarkisov, V., et al. (2019). Observing mesospheric turbulence with specular meteor radars: A novel method for estimating second-order statistics of wind velocity. *Earth and Space Science*, 6, 1171–1195. <https://doi.org/10.1029/2019EA000570>
- Vincent, R. A. (2015). The dynamics of the mesosphere and lower thermosphere: A brief review. *Progress in Earth and Planetary Science*, 2, 4. <https://doi.org/10.1186/s40645-015-0035-8>
- Vincent, R. A., & Reid, I. M. (1983). HF measurements of mesospheric gravity wave momentum fluxes. *Journal of the Atmospheric Sciences*, 40, 1321–1333. [https://doi.org/10.1175/1520-0469\(1983\)040<1321:hdmomg>2.0.co;2](https://doi.org/10.1175/1520-0469(1983)040<1321:hdmomg>2.0.co;2)
- Walterscheid, R. L., & Christensen, A. B. (2016). Low-latitude gravity wave variances in the mesosphere and lower thermosphere derived from SABER temperature observation and compared with model simulation of waves generated by deep tropical convection. *Journal of Geophysical Research: Atmospheres*, 121, 11900–11901. <https://doi.org/10.1002/2016JD024843>
- Wilhelm, S., Stober, G., & Brown, P. (2019). Climatologies and long-term changes in mesospheric wind and wave measurements based on radar observations at high and mid latitudes. *Annals of Geophysics*, 37, 851–875. <https://doi.org/10.5194/angeo-37-851-2019>
- Wright, C. J., Osprey, S. M., & Gille, J. C. (2013). Global observations of gravity wave intermittency and its impact on the observed momentum flux morphology. *Journal of Geophysical Research*, 118, 10–980. <https://doi.org/10.1002/jgrd.50869>
- Wu, D. L. (2001). Horizontal wavenumber spectra of MLS radiance fluctuations. *Journal of Atmospheric and Solar-Terrestrial Physics*, 63, 1465–1477. [https://doi.org/10.1016/S1364-6826\(01\)00025-6](https://doi.org/10.1016/S1364-6826(01)00025-6)
- Yigit, E., Medvedev, A. S., & Ern, M. (2021). Effects of latitude-dependent gravity wave source variations on the middle and upper atmosphere. *Frontiers in Astronomy and Space Sciences*, 7. <https://doi.org/10.3389/fspas.2020.614018>